Draft version March 9, 2023
Typeset using LaTeX **twocolumn** style in AASTeX631

A New Scenario of Solar Modulation Model during the Polarity Reversing

Jieteng Jiang,[1,2] Sujie Lin,[1,2] and Lili Yang[1,2,3]

[1] *School of Physics and Astronomy, Sun Yat-sen University, Guangzhou 510275, People's Republic of China*
[2] *CSST Science Center for Guangdong-Hong Kong-Macau Great Bay Area, Zhuhai 519082, China*
[3] *Department of Physics, University of Johannesburg, PO Box 524, Auckland Park 2006, South Africa*

ABSTRACT

When the Galactic Cosmic Rays (GCRs) entering the heliosphere, they encounter the solar wind plasma, and their intensity is reduced, so called solar modulation. The modulation is caused by the combination of a few factors, such as the particle energies, solar activity and solar disturbance. In this work, a 2D numerical method is adopted to simulate the propagation of GCRs in the heliosphere with SOLARPROP, and to overcome the time consuming issue, the machine learning technique is also applied. With the obtained proton local interstellar spectra (LIS) based on the observation from Voyager 1 and AMS-02, the solar modulation parameters during the solar maximum activity of cycle 24 have been found. It shows the normalization and index of diffusion coefficient indeed reach a maximal value in February 2014. However after taking into account the travel time of particles with different energies, the peak time found postponed to November 2014 as expected. The nine-month late is so called time lag.

Keywords: galactic cosmic ray, AMS-02, machine learning, solar modulation, proton

1. INTRODUCTION

Cosmic rays (GCRs) have been widely studied for more than a hundred years, since the first discovery by Austrian-American physicist Victor Hess. GCRs are charged, energetic nuclei coming from far beyond the solar system, and are believed to be originated from extreme phenomena in the universe. Specifically, GCRs are particles accelerated to high energies from some powerful astronomical objects or magnetic fields in our Milky Way.

When the GCRs cross the heliopause (HP), the boundary of the solar system, they enter the heliosphere where they collide with the solar wind moving outward and are affected by the heliospheric magnetic field (HMF) Parker (1958). As a result, their intensity is modulated, which is varied for different types and energies of particles. This significantly changes their energy spectrum, making it different from the energy spectrum on the boundary, namely the local interstellar spectrum (LIS), especially at lower energies (below 30 GeV). This process is called solar modulation. It encompasses various effects such as diffusion, drift, convection, and adiabatic energy changes (see reviews by e.g. Heber & Potgieter (2006); Moraal (2013); Cliver et al. (2013); Kóta (2013); Potgieter (2013); Engelbrecht et al. (2017)).

The study of solar modulation is essential not only for comprehending the modulation process but also for advancing relevant research. For instance, the study of the transport model of GCR within the Galaxy Yuan et al. (2017) and indirectly searching the dark matter with the anomalous CR antiproton flux Lin et al. (2019) were hindered by the uncertainties in the LIS. A better understanding of the modulation model could help us determine the LIS more accurately and improve these research areas.

Fortunately, we have obtained highly precise GCRs data over several months, which has allowed us to gain a deeper understanding of solar modulation. For example, the Voyager 1 spacecraft, launched in 1977, provided proton data at a few MeV upon crossing heliopause in August 2012 Stone et al. (2013). Additionally, the Alpha Magnetic Spectrometer (AMS-02) has offered precise measurements of protons across a broad energy range of 0.5 GeV to a few TeV Aguilar et al. (2018). We derived the LIS of protons for energy from

Corresponding author: Sujie Lin, Lili Yang
linsj6@mail.sysu.edu.cn, yanglli5@mail.sysu.edu.cn

0.5 GeV to 30 GeV in two periods of low solar activity with interpolating the Voyager 1 data and fitting modulated AMS-02 data Wang et al. (2019, 2022). To numerically describe the instantaneous propagation of GCRs, researchers have widely applied Parker's equation, which is a type of Fokker-Planck equation. With the heliosphere model, solar modulation parameters, and the LIS, the propagation of GCRs can be simulated with tools like SOLARPROP, allowing for the calculation of their energy spectrum at Earth. Fortunately, the physical heliosphere model and the numerical solution to Parker's equation have made significant progress over recent decades (e.g., Fisk (1971); Gleeson et al. (1979); Potgieter & Moraal (1985); Jokipii & Thomas (1981)Potgieter (2000)Potgieter et al. (2014)).

At present, although some results of solar modulation can fit well with data during quiet solar epochs, it remains a challenge during maximum activity. Because it has a more complex coronal structure McComas et al. (2001), and results in the solar wind and HMF behave in a more complicated manner. Nonetheless, some research groups have made progress for the maximum activity period. For example, Song et al. (2021) used five modulation parameters to fit the observed data, Shen et al. (2021) employed a force-field approach to obtain the best-fit parameters, and Fiandrini et al. (2021) introduced a weight to linearly combine of the fluxes with two polarities, and among other methods. In this work, we redefined the weight and considered the differences for particles with varying energies to successfully obtain the best-fit parameters during maximum activity.

This paper is organized as follows. In Section 2, the heliosphere model and diffusion model are described in details. In Section 3, we analyze the cycle 24 data of active periods and apply the machine learning method for better efficiency. In Section 4, the modeling results are given. Also, the LIS of proton and the best-fit parameters from May 2011 to October 2016 are provided. A summary and conclusion are presented in Section 5.

2. NUMERICAL MODEL

To comprehend the solar modulation, the cosmic ray propagation inside the heliosphere has to be understood. When the GCRs enter the solar system, they suffer from energy loss and direction change, which results in a reduction of their intensity. The propagation of these charged particles can be described by the transport equation, which was firstly given by Parker in 1965 Parker (1965) in the form of the Fokker-Planck equation (FPE) without sources

$$\frac{\partial f(\mathbf{r},\mathbf{p},t)}{\partial t} = \nabla(\mathbf{K^S}\cdot\nabla f(\mathbf{r},\mathbf{p},t)) + \frac{1}{3}(\nabla\cdot\mathbf{V_{SW}})\frac{\partial f(\mathbf{r},\mathbf{p},t)}{\partial ln\ p} - (\mathbf{V_{SW}}+\mathbf{V_D})\cdot\nabla f(\mathbf{r},\mathbf{p},t), \tag{1}$$

where $f(\mathbf{r},\mathbf{p},t)$, as a function of position $\mathbf{r}$, momentum $\mathbf{p}$, and temporal variable t, describes the dynamic phase-space distribution of GCRs. On the right side of Equation 1, there are three terms describing the CR transportation processes of diffusion, adiabatic energy loss, and convection and drift in the heliosphere respectively. The physical quantities involved include diffusion coefficient $\mathbf{K^S}$, solar wind velocity $\mathbf{V_{SW}}$ and drift velocity $\mathbf{V_D}$. Here $\mathbf{V_D}$ includes gradient-curvature drift Jokipii et al. (1977); Jokipii & Kopriva (1979) and the heliosphere current sheet (HCS) drift Potgieter & Moraal (1985); Burger & Potgieter (1989); Hoeksema (1992) and diffusion velocity.

To find the solution to FPE, the time-backward numerical method with stochastic differential equations (SDEs) has become popular. Where those pseudo particles are simulated from the moment they reach the earth, and traced backward until they get the heliopause Yamada et al. (1998); Zhang (1999); Kopp et al. (2012); Kappl (2016); Zhang (1999). For a stochastic process driven by Wiener process, the SDEs describe the particle position $d\mathbf{r}$ in the form of,

$$\mathrm{d}\mathbf{r} = (\nabla\cdot\mathbf{K^S}-\mathbf{V})\mathrm{d}t + \overleftrightarrow{\sigma}\cdot\mathrm{d}\mathbf{W}, \tag{2}$$

where $\mathbf{V} = \mathbf{V_{SW}}+\mathbf{V_D}$ is the global velocity of the particles, $\overleftrightarrow{\sigma}$ is a third-order matrix satisfying $\overleftrightarrow{\sigma}\cdot\overleftrightarrow{\sigma} = 2\mathbf{K^S}$, $\mathrm{d}\mathbf{W}$ is a Wiener process related to a standard normal distribution $N(0,1)$. The kinetic energy $\mathrm{d}T$ of a cosmic ray particle with mass m in $\mathrm{d}t$ time interval can be found as

$$\mathrm{d}T = \frac{2|\mathbf{V_{SW}}|}{3|\mathbf{r}|}\frac{T^2+2Tm}{T+m}\mathrm{d}t, \tag{3}$$

here m is the mass of particle. With the constructed numerical method above, we adopted the public code SOLARPROP Kappl (2016) to perform the simulation. Based on this framework, one can change the propagation model according to various presumptions on the physical quantities. In this work, we adopted a 2D model to describe these quantities inside the heliosphere following Ref. Potgieter et al. (2014).

2.1. *Heliosphere Model*

Both the diffusion coefficient $\mathbf{K^S}$ and the drift velocity $\mathbf{V_D}$ depend on the HMF and solar wind. Previously the large-scale HMF, embedded into the outward-flowing solar wind, was given by Parker as an Archimedean spiral

field Parker (1958). However, as the transverse component of the HMF decreases as $1/r$ while the radial component decreases as $1/r^2$, the transverse perturbation near the sun would significantly enhance the average magnitude of the magnetic field in the polar region Jokipii & Kota (1989). In this work, we adopt the HMF model performed in Ref. Fichtner et al. (1996), which takes the transverse perturbation into account by modifying the magnitude of the Archimedean spiral field. This modification is supported by measurements of the magnetic field in the polar regions of the heliosphere by Ulysses Balogh et al. (1995). The modified HMF model can be written in the form

$$\begin{cases} \boldsymbol{B} = A\ B_0 \dfrac{r_0^2}{r^2}(\boldsymbol{e_r} + \zeta \boldsymbol{e_\theta} - \psi \boldsymbol{e_\varphi}) \\ \zeta = \dfrac{r\delta(\theta)}{r_\odot sin(\theta)} \\ \psi = \dfrac{\Omega(r - r_\odot)sin(\theta)}{V_{SW}} \end{cases} \tag{4}$$

where $\Omega = 2.7 \times 10^{-6}$rad/s is the rotation angular velocity of the sun, $r_\odot = 3 \times 695500$ km is the radius of the corona, V_{SW} is the velocity of the solar wind, B_0 is the HMF observed at the reference point r_0, A is the polarity of the field and could only be 1 or -1, the N pole of HMF locate in the northern solar hemisphere in the case $A = 1$ and vice verse, and $\delta(\theta)$ is presumed to follow the expression Fiandrini et al. (2021)

$$\delta(\theta) = \begin{cases} 3 \times 10^{-3} \sin(\theta), & 1.7^\circ < \theta < 178.3^\circ \\ 8.7 \times 10^{-5}, & \text{else} \end{cases}. \tag{5}$$

The observation shows that the solar wind speed $\mathbf{V_{SW}}$ changes with radial and polar position, during periods of minimum solar activity Bame et al. (1992); Heber & Potgieter (2006). Along the radial direction of the equatorial plane, the wind speed keeps constant at 430 km/s until reaching the termination shock (TS). It decreases to about 170 km/s after across the TS and finally becomes zero or moves to tail-ward in the inner heliosheath because of the barrier of the heliopause (HP) Krimigis et al. (2011). While in the polar direction, $\mathbf{V_{SW}}$ increases from about 430 km/s to 800 km/s at high polar region, as observed by Heber & Potgieter (2006). The solar wind speed was given by Potgieter et al. (2014),

$$\begin{aligned} \mathbf{V_{SW}}(r,\theta) =& V_0(1.475 \mp 0.4 \tanh[6.8(\theta - \frac{\pi}{2}) \pm (\frac{15\pi}{180} + \alpha)]) \\ & \times [\frac{s+1}{2s} - \frac{s-1}{2s} \tanh(\frac{r - r_{TS}}{L})]\boldsymbol{e_r} \end{aligned} \tag{6}$$

where $V_0 = 400$ km/s, θ is the polar angle, the distance of termination shock $r_{TS} = 90$ AU, $s = 2.5$ and $L = 1.2$ AU. And α is the tilt angle that describes the angle of the HCS. For the same θ, the radial variation of Equation 6 is a constant while the polar variation changes from 430 km/s near the equator to 800 km/s in the polar region. The HMF strength around the earth B_0, polarity A, and the tilt angle α in Equation 4 and 6 have to be obtained from the observation.

2.2. *Diffusion Model*

In Equation 1, the spatial diffusion coefficient tensor $\mathbf{K^S}$ describes the diffusion of GCRs. In general, the full diffusion tensor is expressed as $\mathbf{K} = \mathbf{K^S} + \mathbf{K^A}$. It includes symmetric diffusion tensor $\mathbf{K^S}$, which is diagonal, and asymmetric diffusion tensor $\mathbf{K^A}$ as following,

$$\begin{aligned} \mathbf{K} = \begin{bmatrix} K_{r\perp} & -K_A & 0 \\ K_A & K_{\theta\perp} & 0 \\ 0 & 0 & K_\parallel \end{bmatrix} = & \underbrace{\begin{bmatrix} K_{r\perp} & 0 & 0 \\ 0 & K_{\theta\perp} & 0 \\ 0 & 0 & K_\parallel \end{bmatrix}}_{\mathbf{K^S}} \\ & + \underbrace{\begin{bmatrix} 0 & -K_A & 0 \\ K_A & 0 & 0 \\ 0 & 0 & 0 \end{bmatrix}}_{\mathbf{K^A}} \end{aligned} \tag{7}$$

The symmetric part describes the normal diffusion effect while the asymmetric part describes the drift effect. The symmetric part, $K_\parallel$, is the diffusion component parallel to the direction of the magnetic field, $K_{r\perp}$ and $K_{\theta\perp}$ are two perpendicular diffusion coefficients in the radial direction and the polar direction respectively. A typical empirical expression for the $K_\parallel$ is given by Ref. Potgieter et al. (2014) in the form of

$$K_\parallel = (K_0)\,\beta \left(\frac{B_0}{|\mathbf{B}|}\right) \left(\frac{R}{R_0}\right)^a \left(\frac{\left(\frac{R}{R_0}\right)^m + \left(\frac{R_k}{R_0}\right)^m}{1 + \left(\frac{R_k}{R_0}\right)^m}\right)^{\frac{b-a}{m}}, \tag{8}$$

where K_0 is a constant with an order of $10^{23}\mathrm{cm^2 s^{-1}}$, $\beta = v/c$ is the speed of the particle in the nature unit, B_0 is the value of HMF detected around the Earth, $R = p/Z$ is the particle rigidity, the reference rigidity $R_0 = 1$ GV, and $m = 3.0$ guarantees the smoothness of the transition. The indexes a and b determine the slope of the rigidity dependence respectively below and above a rigidity with the value $R_k = 3$ GV.

Perpendicular diffusion term in the radial direction is presumed to Giacalone & Jokipii (1999)

$$K_{r\perp} = 0.02\ K_\parallel, \tag{9}$$

while the polar perpendicular diffusion term is given as Ref. Potgieter (2000); Balogh et al. (2008)

$$K_{\perp\theta} = 0.02 K_{\parallel} f_{\perp\theta}. \tag{10}$$

The factor $f_{\perp\theta}$ satisfies the expression

$$f_{\perp\theta} = A^{+} \mp A^{-} \tanh[8(\theta_A - 90^\circ \pm \theta_F)], \tag{11}$$

where $A^{\pm} = (d \pm 1)/2$, $\theta_F = 35^\circ$, and $\theta_A = 90^\circ - |90^\circ - \theta|$. This means that $K_{\perp\theta}$ is enhanced towards the poles by a factor of d with respect to the value of $K_{\parallel}$ in the equatorial regions of the heliosphere. The enhance factor d is set to be 3.

Plugging the asymmetric part into the diffusion term $\nabla(\mathbf{K^A} \cdot \nabla f)$ would lead to a cross-product-like result in the form of $\nabla \times \mathbf{B} \cdot \nabla f$. This term could describe the drift effect caused by the uneven magnetic field, thus it was written as the drift velocity in Equation 1. Under the assumption of weak scattering and full drift process, the average drift velocity is related to the rigidity R and the charge q of particles, and the strength of magnetic field B Burger et al. (1985, 1987):

$$\langle \mathbf{V_D} \rangle = \nabla \times (\frac{qR\beta}{3B} \frac{\mathbf{B}}{B})). \tag{12}$$

The drift velocity can be divided into two parts, gradient-curvature drift velocity $\mathbf{V_G}$ from the magnetic field itself and HCS drift velocity $\mathbf{V_{HCS}}$ from the HCS. The two drift velocities are expressed with two factors, $f(\theta)$ and $\zeta(R)$, given as Potgieter & Moraal (1985); Burger et al. (2000),

$$\begin{cases} \mathbf{V_G} = f(\theta)\zeta(R) \cdot \nabla \times (\frac{qR\beta}{3B} \frac{\mathbf{B}}{B}) \\ \mathbf{V_{HCS}} = \zeta(R) \frac{qR\beta}{3B} \frac{\mathbf{B}}{B} \nabla \times f(\theta) \\ f(\theta) = \frac{1}{\alpha_h} \tan^{-1}[(1 - \frac{2\theta}{\pi}) \tan \alpha_h] \\ \zeta(R) = \frac{(R/R_A)^2}{1 + (R/R_A)^2} \end{cases}. \tag{13}$$

Here the cut-off value R_A is fixed to be 0.5 GV according to Fiandrini et al. (2021), $f(\theta)$ is a transition function that models a wavy neutral sheet near the equator plane. And $\zeta(R)$ is a reduction function, which describes the change of drift velocity for particles with different momentum. The angle α_h equals to $arccos(\frac{\pi}{2c_h} - 1)$, here $c_h = \frac{\pi}{2} - \frac{1}{\pi} sin(\alpha + \frac{2r_L}{r})$, α is tilt angle and r_L depends on the maximum distance that particle can be away from the HCS.

In summary, the diffusion coefficient has been well established with our assumptions, except the three parameters, K_0, indices a and b, which are obtained from the analysis of the experiment data.

3. ANALYSIS AND CALCULATION

3.1. *The Model Parameters*

To calculate the spectrum of GCRs using the heliosphere model and the diffusion model, six parameters are required, which consist of three heliospheric parameters related to the solar system and three diffusion parameters. The heliospheric parameters are the strength B_0 of the HMF near the Earth, the tilt angle α of the HCS, and the polarity A of the HMF, which can be obtained from observations, as shown in Figure 1. The value of B_0 is provided by the Advanced Composition Explorer (ACE), while the tilt angle and polarity are provided by the Wilcox Solar Observatory (WSO), represented by solid lines in the two top panels. It takes time for the change in the magnetic field that embedded in the solar wind to affect the motion of GCR, typically around nine months, which is referred to as the time lag Tomassetti et al. (2017); Orcinha et al. (2019). Considering that, we calculate the average field and tilt angle encountered by GCR particles during their journey from heliopause to Earth, as represented by the square symbol. The last panel in Figure 1 shows the sunspot number (SSN) as a reference to compare the trend of B_0 and α. It can be observed that B_0 and α increase with SSN, which reaches maximum values in February 2014, and the polarity reverses around this time. Other three diffusion parameters (normalization factor of diffusion K_0 and two spectral indices a and b in Equation 8) can be obtained by fitting the observed data.

3.2. *Application of Machine Learning*

In this work, we applied the heliospheric model as described in Section 2 and utilized SOLARPROP to simulate the propagation of GCR. SOLARPROP simulates the propagation of particles in the heliosphere. There are 30 energy bins and each has 2000 particles, starting from the earth. On average, it takes 1500 steps for one particle to reach the HP. Therefore a total of billions of steps are taken for all particles, and it needs about 10 minutes for SOLARPROP to complete one simulation. Running thousands of simulations can be quite time-consuming. To improve efficiency, we employed a machine learning method, the LIBSVM library of Support Vector Machine (SVM) Chang & Lin (2011), to replace the calculations of SOLARPROP. In order to construct the SVM model, we set a 5D parameter space with the following ranges:

- B_0 in the range of $(3 \sim 8)$nT
- α in the range of $15^\circ \sim 75^\circ$
- K_0 in the range of $(0.001 \sim 1.5) \times 10^{23}\mathrm{cm^2 s^{-1}}$

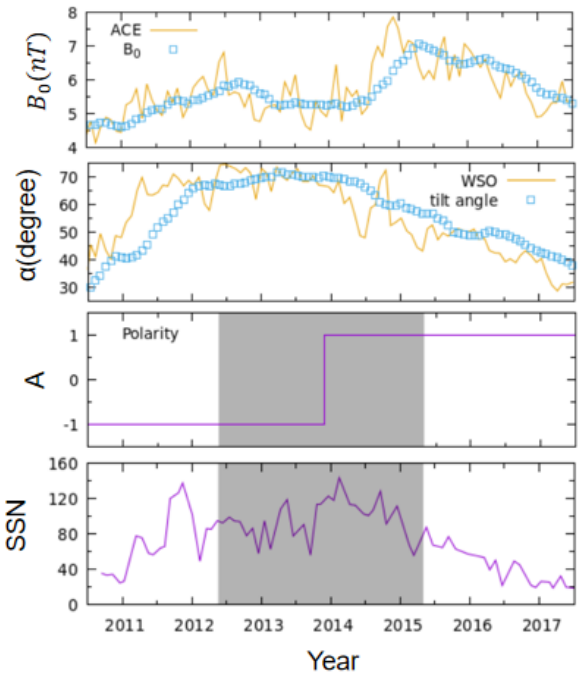

Figure 1. The observed data (solid line) of HMF B_0, tilt angle α, polarity A and sunspot number from the Advanced Composition Explorer (ACE) and the Wilcox Solar Observatory (WSO), separately, from 2011 to 2017. The square symbols are the average parameters of the ten periods of carrington rotation numbers. In the last two panels, the shaded regions represent the period from May 2012 to March 2015.

- the indices a and b in the range of $0.001 \sim 3$

We randomly picked about 40000 samples for $A = 1$ and about 50000 samples for $A = -1$ from this parameter space to train the SVM model. To ensure the reliability of the machine learning method, we performed detailed tests in Section 4.1.

3.3. *Analysis for Solar Cycle 24*

In a recent study of the solar polar magnetic field during the activity maximum in cycle 24, researchers observed that the magnetic field underwent three reversals in the northern hemisphere (in May 2012, February 2014, and July 2014) and only one reversal in the southern hemisphere (in November 2013). This asymmetry of the magnetic field reversals has created a challenge in simulating solar modulation during this period, as the particles will experience magnetic fields with different signs. To address this issue, various methods have been proposed, such as adding more modulation parameters (as done by Song et al. (2021)) or simplifying the particle flux as a weighted sum of two spectra with different polarities (as proposed by Fiandrini et al. (2021)). We adopt the latter method and give the weight a physical meaning, as the ratio of the space occupied by the N-pole magnetic field in the heliosphere to the total space. Meanwhile, we also take into account the different motion times of particles with different energies.

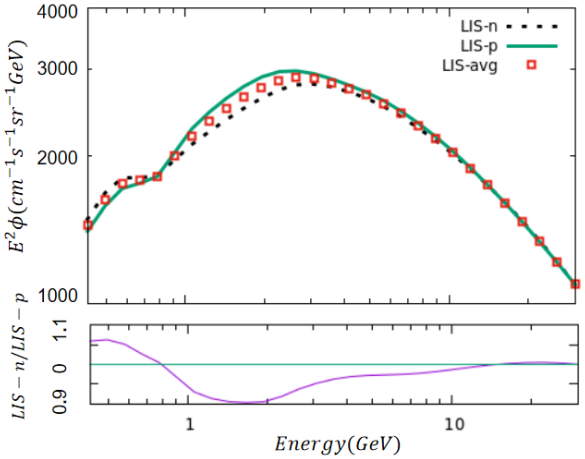

Figure 2. Derived the best-fit LIS of proton, constrained by the data from Voyager 1 and AMS-02. In the upper panel, LIS-n/LIS-p with negative/positive polarity are shown in dotted/solid lines, and the average LIS of LIS-n and LIS-p, labeled by LIS-avg. The ratio of LIS-n to LIS-p is shown in the second panel.

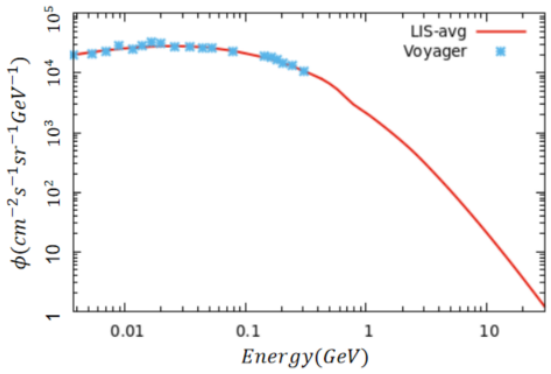

Figure 3. LIS-avg comparing with Voyager data in heliopause are shown in square symbols.

4. RESULTS

4.1. *The Local Interstellar Spectrum of proton*

The local interstellar spectrum (LIS) of protons represents the energy spectrum outside the heliopause. Voyager 1 crossed the heliopause in August 2012 and provided the LIS for protons at low energy (< 0.5 GeV). Additionally, energy spectra above a few GeV were measured by AMS-02 near the Earth. Solar modulation effects are significant below 30 GeV, but no observed LIS of protons has been obtained in the energy range

Figure 4. The time profile of the difference between ϕ_{prop} and ϕ_{svm}, calculated from SOLARPRO and Libsvm, to the total err of AMS-02.

between 0.4 GeV and 30 GeV. Therefore, the LIS in this range needs to be calculated. With cubic spline interpolation, a complete LIS is obtained that considers the constraints from Voyager 1 observations and fits the AMS-02 data after solar modulation.

To study the LIS, the proton data observed by AMS-02 from two quiet periods were chosen, which corresponded to Bartels' numbers 2426-2437 and 2470-2487, respectively, and corresponded to different HMF polarities. Two independent fittings were performed, and two proton LIS were obtained for the two periods (in Figure 2), named LIS-n (dotted line) for negative polarity and LIS-p (solid line) for positive polarity. These two LIS are quite close, with a relative difference of less than 10%. It is well known that cosmic ray particles propagate in different paths for different HMF polarities due to the drift direction. A positive charge particle is likely to propagate inward along the heliospheric current sheet (HCS) in the negative polarity period, while it is likely to propagate along the polar regions in the positive polarity period. The reverse applies for the negative charge particle. The two LIS were averaged to obtain a unified LIS (LIS-avg) for the following work, which is shown as square symbols in Figure 3.

To evaluate the validity of machine learning, SOLARPROP and LIBSVM were applied with given LIS-n and LIS-p, and the fluxes ϕ_{svm} and ϕ_{prop} were obtained after solar modulation using best-fit parameters for every energy bin. By comparing the difference between ϕ_{prop} and ϕ_{svm} and the total error of AMS-02, the validity is given in Figure 4. The ratio are mostly less than one for both LIS-n and LIS-p, which means the difference between ϕ_{prop} and ϕ_{svm} from the two methods is smaller than the total error and can be neglected in our analysis.

4.2. *Quiet Periods*

To determine the best-fit parameters for cycle 24 during solar maximum activity, we analyzed the full set of data from May 2011 to October 2016. In this data set, we bin the data into 34 energy bins from 0.47 GeV to 24.71 GeV, namely the degree of freedom is 34. The resulting values for the parameters K_0, a, and b are presented in Figure 5. Notably, two parameters, K_0 and index a, exhibit a sudden change in November 2013. Specifically, the diffusion coefficient K_0 decreases, while index a increases. This change can be attributed to the polarity shift illustrated in the third panel of Figure 1. In contrast, the value of index b remained stable throughout the analyzed period.

As seen the last panel in Figure 5, the value of reduced chi square is less than 1 during two quiet periods. But the value increases to more than 1 and keep on for a long time, the increasing rate is more than 60%, the time nodes are May 2012 and May 2015. So we think that the solar magnetic field reversal occurred from May 2012 to May 2015. Some other works also hold the same point, like Pishkalo & Leiko (2016); Gopalswamy et al. (2016) through the observed polar magnetic field on surface of the Sun. Even though the polar field observations(above 55°) from the Wilcox Solar Observatory in Figure 6, the first time change of the polar magnetic field in the northern hemisphere was June 2012, and the last time was August 2014. After we added the time lag of surface magnetic field, nine months, it is just in May 2015.

For high values of reduced χ^2 (> 2) in the last panel of Figure 5, especially the period from December 2013

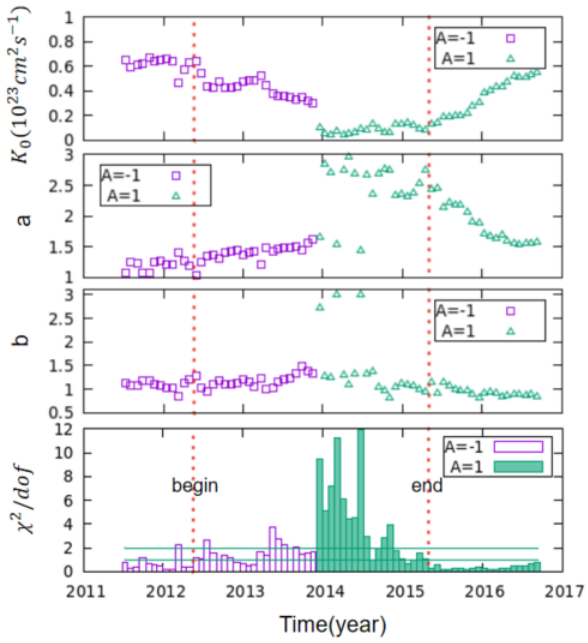

Figure 5. Results of the best-fit parameters, K_0, a and b for two periods, $A = -1$ (square) and $A = 1$ (triangle), and the corresponding reduced chi square in the last panel, here the dof equals to 34. The vertical dashed lines indicate the beginning and the end of the reversal epoch.

to November 2014, we think that three diffusion model parameters can not fit the observed data. Therefore we think to get more reasonable results, these data have to be analysed with other methods during this maximum activity period.

4.3. *Maximum Activity*

During periods of maximum activity, the sign of the large-scale magnetic field can vary at different positions, even within the same hemisphere. As a result, cosmic rays will encounter the HMF with different polarities along their path. Ideally, the magnetic field at the location of each cosmic ray should be simulated, but currently, it is not possible to detect the magnetic polarity and path of every cosmic ray within the heliosphere. Nonetheless, some progress has been made in simplifying this process. For example, Fiandrini et al. (2021) introduced a weight term, denoted by P, to calculate the final spectrum, ϕ_f near the Earth. This spectrum is the weighted sum of the spectra with two polarities, $\phi^-(E)$ with $A = -1$, and $\phi^+(E)$ with $A = 1$.

$$\phi_f(E) = \phi^-(E)(1 - P) + \phi^+(E)P \qquad (14)$$

Here we employ a similar approach. Considering that magnetic field transports at solar wind speeds, we define

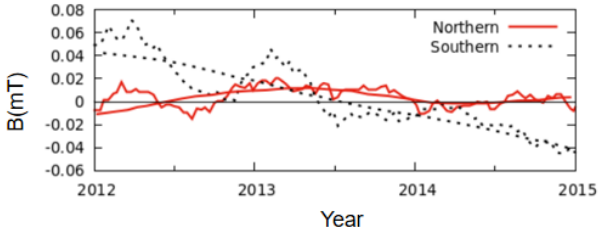

Figure 6. The two polar magnetic fields (above 55°), northern pole (solid line) and southern pole (dotted line). The wave line is 10 days averaged, Data is from the Wilcox Solar Observatory.

the weight as the ratio of the space occupied by the N-pole magnetic field in the heliosphere to the total space. Figure 6 shows that the directions of the polar magnetic field (above 55°) have changed over time for both the northern and southern hemispheres. The northern hemisphere experienced magnetic field reversals three times in May 2012, February 2014, and August 2014, while the southern hemisphere experienced one in July 2013. The calculated weight is presented in the forth panel of Figure 7, where two structures, platform A and valley B, are evident. These structures can be explained by the temporary stability of the solar field in the first half of 2013 and the change to a negative field in the northern hemisphere in the first half of 2014. Using the specified weight, the best-fit parameters are shown in the first three panels in Figure 7, where the parameters change continuously. The parameter K_0 gets at a minimum in February 2014, and the index a reaches a maximum at the same time. When compared to the SSN change in Figure 1, which also reaches an extreme value in February 2014, the parameters show obvious trends with the change in solar activity. However, although these three parameters show clear trends, the reduced χ^2 in the last panel of Figure 7 still has a high value, especially from August 2014 to April 2015, making the results somewhat unsatisfactory. Thus, further improvement is necessary.

To improve our results, we take into account the different traveling times of GCRs with different energies. To achieve this, we have utilized the time data simulated by SOLARPROP as a reference, which provides the proton traveling time for each energy level. We have used the average values of parameters such as $K_0 = 0.3 \times 10^{23} cm^{-2} s^{-1} sr^{-1} GeV^{-1}$, $a = 1.80$, $b = 0.989$, $B_0 = 5nT$, $\alpha = 70°$, and $A = 1$. These values have been selected based on the points with χ^2/dof greater than 1 in the last panel of Figure 7. The time range for each energy bin is between 1.87 and 163 days, and particle travel time decreases as their energy increases. By adding this information, the best-fit param-

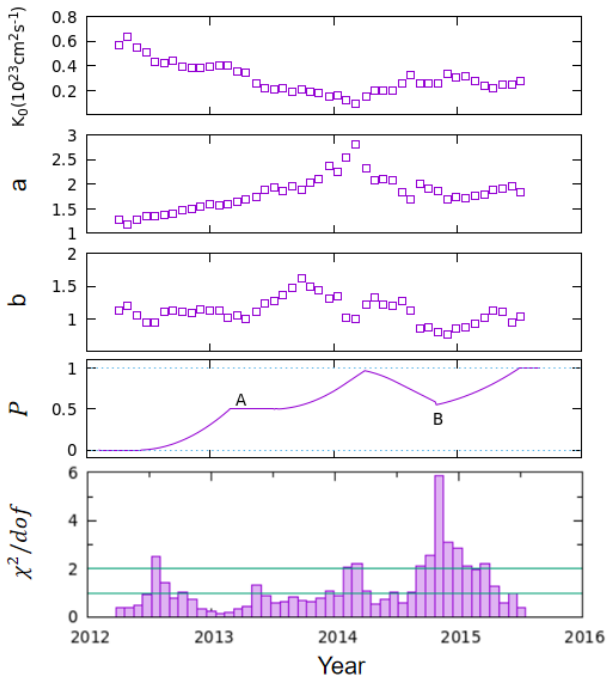

Figure 7. The best-fit parameters during maximum activity from May 2012 to May 2015. The final flux near the Earth is the weighted sum of the spectra with two polarities. The weight P is the ratio of the space occupied by the N-pole magnetic field in the heliosphere to the total space, shown in the forth panel. The reduced χ^2 is in the last panel

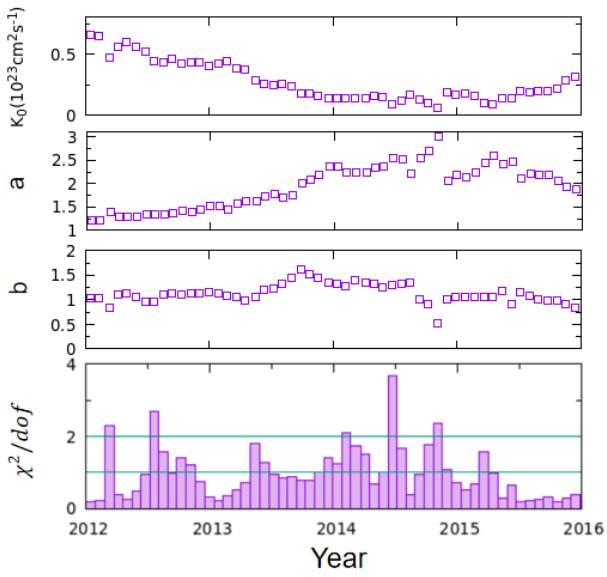

Figure 8. The best-fit parameters during maximum activity considering different traveling times of GCRs with different energies in the first three panel. The reduced χ^2 is in the last panel

eters and reduced χ^2 are shown in Figure 8. The three diffusion parameters have the same trends as shown in Figure 7, but the extreme values are in November 2014, and the index b is stable as always. Compared with the time reaching extreme values in Figure 7, the difference of time is nearly 9 months, which is just a time lag. The reduced χ^2 in the last panel of Figure 8 shows that 60% of them have a value less than 1, 90% less than 2, and only one has a maximum of 3.7. Therefore, we conclude that these best-fit parameters are reliable.

5. CONCLUSION

This study examines the solar modulation of Galactic Cosmic Rays (GCRs) and presents a new Local Interstellar Spectrum (LIS) of protons during solar activity in cycle 24, as seen in Figure 3. The final spectrum near the Earth during the period of maximum solar activity is obtained using a weight factor in Equation 14, which is defined as the ratio of the space occupied by the N-pole magnetic field in the heliosphere. The weight factor is used to fit the final spectrum, which is equal to a weighted sum of two spectra with both polarities. The best-fit diffusion parameters are then determined, and their trends are shown in Figure 7. The normalization diffusion coefficient K_0 reached a minimum in February 2014, while index a reached its maximum at the same time. In contrast, index b does not exhibit a regular change. However, due to the different motion times of particles with different energies in space, the ratio of the magnetic field occupying needs to be modified for each particle. The modified best-fit parameters are shown in Figure 8, which also have one extreme point, but this time it is in November 2014, nine months later than before. This delay time represents the time taken for the solar magnetic field to act on the energy spectrum, namely the time lag.

The time lag was discussed with different methods in the literature. For example, the Ref. Fiandrini et al. (2021), in which the weight during the maximum solar activity period was described in a different way from us, established a relationship between the parameters and the sunspot number (SSN) at the epoch $t - \Delta T_{lag}$, and found that the curve of K_0 vs SSN approaches a single-valued function. The ΔT_{lag} finally given by this method is about 11 months, which is comparable with the 9 months in our study.

To improve the reliability of LIS in future work, there are two main steps that should be taken. Firstly, it is important to overlap the energy range between Voyager data and that near the earth. Currently, the AMS-02 data is used, but there is no overlapped energy range between the Voyager and AMS-02 data. To address this issue, data from PAMELA can be utilized. The energy

range of PAMELA data is ($0.088 \sim 46.5$GeV), which covers the energy range of interest. However, PAMELA data is only available during negative polarity, which limits the ability to obtain the LIS with positive polarity. Therefore, it is necessary to wait for PAMELA to release new observations. Secondly, to account for the difference in particle motion time, it is important to consider the motion time of particles corresponding to diffusion parameters rather than the average parameters. By doing so, the reliability of the results can be improved. In summary, the two next steps to improve the reliability of LIS are to utilize PAMELA data and to consider the motion time of particles corresponding to diffusion parameters.

6. ACKNOWLEDGEMENTS

We thank E. Fiandrini and N. Tomassett for the valuable discussion with them. This work is supported by the National Natural Science Foundation of China (NSFC) grants 12205388, 12005313, 42150105, and 12261141691.

REFERENCES

Aguilar, M., Cavasonza, L. A., Alpat, B., et al. 2018, Physical review letters, 121, 051101

Balogh, A., Lanzerotti, L. J., Suess, S. T., Heber, B., & Potgieter, M. 2008, The heliosphere through the solar activity cycle, 195

Balogh, A., Southwood, D., Forsyth, R., et al. 1995, Science, 268, 1007

Bame, S., McComas, D., Barraclough, B., et al. 1992, Astronomy and Astrophysics Supplement Series (ISSN 0365-0138), vol. 92, no. 2, Jan. 1992, p. 237-265. Research supported by DOE., 92, 237

Burger, R., Moraal, H., & Potgieter, M. 1987, in International Cosmic Ray Conference, Vol. 3, 283

Burger, R., Moraal, H., & Webb, G. 1985, Astrophysics and space science, 116, 107

Burger, R., & Potgieter, M. 1989, The Astrophysical Journal, 339, 501

Burger, R., Potgieter, M., & Heber, B. 2000, Journal of Geophysical Research: Space Physics, 105, 27447

Chang, C.-C., & Lin, C.-J. 2011, ACM Trans. Intell. Syst. Technol., 2, 27:1, doi: 10.1145/1961189.1961199

Cliver, E. W., Richardson, I. G., & Ling, A. G. 2013, Space Sci. Rev., 176, 3, doi: 10.1007/s11214-011-9746-3

Engelbrecht, N., Strauss, R., Le Roux, J., & Burger, R. 2017, The Astrophysical Journal, 841, 107

Fiandrini, E., Tomassetti, N., Bertucci, B., et al. 2021, Physical Review D, 104, 023012

Fichtner, H., Sreenivasan, S., & Fahr, H. 1996, Astronomy and Astrophysics, v. 308, p. 248-260, 308, 248

Fisk, L. A. 1971, Journal of Geophysical Research, 76, 221

Giacalone, J., & Jokipii, J. 1999, The Astrophysical Journal, 520, 204

Gleeson, L., Moraal, H., & Webb, G. 1979, in International Cosmic Ray Conference, Vol. 3, 1

Gopalswamy, N., Yashiro, S., & Akiyama, S. 2016, The Astrophysical Journal Letters, 823, L15

Heber, B., & Potgieter, M. 2006, Space Science Reviews, 127, 117

Hoeksema, J. 1992, in Solar wind seven (Elsevier), 191–196

Jokipii, J., & Kopriva, D. A. 1979, Astrophysical Journal, Part 1, vol. 234, Nov. 15, 1979, p. 384-392., 234, 384

Jokipii, J., & Kota, J. 1989, Geophysical Research Letters, 16, 1

Jokipii, J., Levy, E., & Hubbard, W. 1977, The Astrophysical Journal, 213, 861

Jokipii, J., & Thomas, B. 1981, The Astrophysical Journal, 243, 1115

Kappl, R. 2016, Computer Physics Communications, 207, 386

Kopp, A., Büsching, I., Strauss, R., & Potgieter, M. 2012, Computer Physics Communications, 183, 530

Kóta, J. 2013, Space Science Reviews, 176, 391

Krimigis, S. M., Roelof, E. C., Decker, R. B., & Hill, M. E. 2011, Nature, 474, 359

Lin, S.-J., Bi, X.-J., & Yin, P.-F. 2019, Phys. Rev., D100, 103014, doi: 10.1103/PhysRevD.100.103014

McComas, D., Goldstein, R., Gosling, J., & Skoug, R. 2001, Space Science Reviews, 97, 99

Moraal, H. 2013, Space Science Reviews, 176, 299

Orcinha, M., Tomassetti, N., Barão, F., & Bertucci, B. 2019, Journal of Physics: Conference Series, 1181, 012013, doi: 10.1088/1742-6596/1181/1/012013

Parker, E. 1965, Planetary and Space Science, 13, 9, doi: https://doi.org/10.1016/0032-0633(65)90131-5

Parker, E. N. 1958, The Astrophysical Journal, 128, 664

Pishkalo, M., & Leiko, U. 2016, Kinematics and Physics of Celestial Bodies, 32, 78

Potgieter, M., & Moraal, H. 1985, The Astrophysical Journal, 294, 425

Potgieter, M., Vos, E., Boezio, M., et al. 2014, Solar Physics, 289, 391

Potgieter, M. S. 2000, Journal of Geophysical Research: Space Physics, 105, 18295

—. 2013, Living Reviews in Solar Physics, 10, 1

Shen, Z., Yang, H., Zuo, P., et al. 2021, The Astrophysical Journal, 921, 109

Song, X., Luo, X., Potgieter, M. S., Liu, X., & Geng, Z. 2021, The Astrophysical Journal Supplement Series, 257, 48

Stone, E., Cummings, A., McDonald, F., et al. 2013, Science, 341, 150

Tomassetti, N., Orcinha, M., Barão, F., & Bertucci, B. 2017, Astrophys. J. Lett., 849, L32, doi: 10.3847/2041-8213/aa9373

Wang, B.-B., Bi, X.-J., Fang, K., Lin, S.-J., & Yin, P.-F. 2019, Physical Review D, 100, 063006

—. 2022, Physical Review D, 106, 063006

Yamada, Y., Yanagita, S., & Yoshida, T. 1998, Geophysical research letters, 25, 2353

Yuan, Q., Lin, S.-J., Fang, K., & Bi, X.-J. 2017, Phys. Rev., D95, 083007, doi: 10.1103/PhysRevD.95.083007

Zhang, M. 1999, The Astrophysical Journal, 513, 409